ADVANCED FUNCTIONAL MATERIALS
www.afm-journal.de

Dual Role of Subphthalocyanine Dyes for Optical Imaging and Therapy of Cancer

Eveline van de Winckel, Marta Mascaraque, Alicia Zamarrón, Ángeles Juarranz de la Fuente, Tomás Torres,* and Andrés de la Escosura**

The family of subphthalocyanine (SubPc) macrocycles represents an interesting class of nonplanar aromatic dyes with promising features for energy conversion and optoelectronics. The use of SubPcs in biomedical research is, on the contrary, clearly underexplored, despite their documented high fluorescence and singlet oxygen quantum yields. Herein, for the first time it is shown that the interaction of these chromophores with light can also be useful for theranostic applications, which in the case of SubPcs comprise optical imaging and photodynamic therapy (PDT). In particular, the article evaluates, through a complete in vitro study, the dual-role capacity of a novel series of SubPcs as fluorescent probes and PDT agents, where the macrocycle axial substitution determines their biological activity. The 2D and 3D imaging of various cancer cell lines (i.e., HeLa, SCC-13, and A431) has revealed, for example, different subcellular localization of the studied photosensitizers (PS), depending on the axial substituent they bear. These results also show excellent photocytotoxicities, which are affected by the PS localization. With the best dual-role PS, preliminary in vivo studies have demonstrated their therapeutic potential. Overall, the present paper sets the bases for an unprecedented biomedical use of these well-known optoelectronic materials.

1. Introduction

The integration of therapeutics and diagnostics, also called theranostics, represents a major goal of current biomedical research, which pursues to achieve more site-specific, efficient, and personalized healthcare.[1,2] A straightforward approach toward this goal involves the use of theranostic agents that comprise the therapeutic and diagnostic functions within a single molecular framework. Optical imaging and therapy methods are becoming indispensable in this respect, as they allow tuning both kinds of functions through designed interactions of the theranostic agent with light.[3] Compared to other imaging modalities, fluorescence imaging presents various advantages such as its noninvasive character, subcellular spatial resolution, high temporal resolution, and high sensitivity in the detection of biological structures at low concentration levels.[4] Photodynamic therapy (PDT),[5] on the other hand, is a clinically approved form of phototherapy that makes use of nontoxic photoactive compounds, called photosensitizers (PS). When exposed selectively to light of a certain wavelength, PS become toxic to targeted malignant and other diseased cells or microorganisms,[6] through the generation of singlet oxygen ($^1O_2$) and reactive oxygen species (ROS).[7] Importantly, integrating fluorescence emission with the capacity to convert light into $^1O_2$ and ROS yields PS that can perform as both imaging and PDT agents.[8,9] However, there are few examples of PS with optimum emission features for use as fluorescent probes, and vice versa. In this respect, herein we report for the first time on the promising dual-role of subphthalocyanine dyes for optical imaging and therapy of cancer.

Subphthalocyanines (SubPcs) form part of the pyrrolic macrocycle family, and comprise a 14-π electron aromatic structure with C_3 symmetry, formed by three isoindole units linked through aza bridges around a tetracoordinated boron atom.[10] They are considered lower homologs of Pcs,[11–15] which constitute one of the most important families of PS.[16–21] In contrast to Pcs, SubPcs present a conical π surface, which renders them with excellent properties for photovoltaic and optoelectronic applications,[22] such as a lower tendency to aggregation and the possibility to tune them through axial substitution. Such features, in combination with the intense absorption and emission of SubPcs close to the therapeutic window (at ≈560 and 570 nm, respectively), also enable their use in biomedical research, yet the number of reports about these nonplanar chromophores in the context of fluorescence imaging[23–25] or PDT[26,27] remain extremely scarce. In this respect, both the well-known high SubPc fluorescence and $^1O_2$ quantum yields (ϕ_F = 0.2–0.9 and ϕ_Δ = 0.5–0.7, respectively)[28–30] prompted us to explore the

Dr. E. van de Winckel, Prof. T. Torres, Dr. A. de la Escosura
Departamento de Química Orgánica
Universidad Autónoma de Madrid
Madrid 28049, Spain
E-mail: tomas.torres@uam.es; andres.delaescosura@uam.es
Prof. T. Torres, Dr. A. de la Escosura
Institute for Advanced Research in Chemical Sciences (IAdChem)
UAM
Madrid 28049, Spain
M. Mascaraque, Dr. A. Zamarrón, Prof. Á. Juarranz de la Fuente
Departamento de Biología
Universidad Autónoma de Madrid
Madrid 28049, Spain
E-mail: angeles.juarranz@uam.es
The ORCID identification number(s) for the author(s) of this article can be found under https://doi.org/10.1002/adfm.201705938.

DOI: 10.1002/adfm.201705938

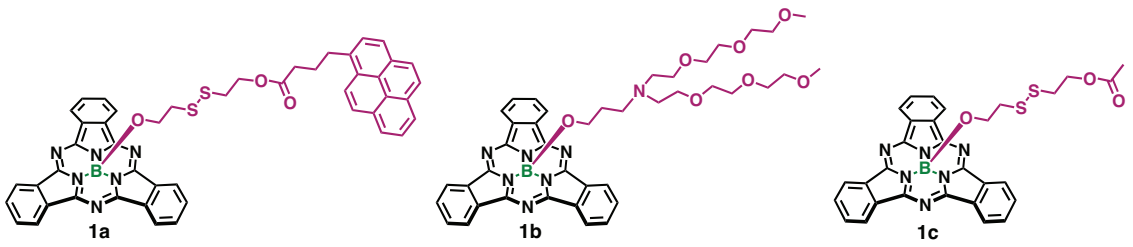

Figure 1. Chemical structure of the series of SubPc derivatives **1a–c**.

potential dual functioning of these dyes as fluorescent probes and PS for PDT.

The series of SubPc derivatives (**1a–c**, **Figure 1**) under study presents different substituents at the apical position of the boron atom, which allows tuning the balance between hydrophilicity and hydrophobicity of the PS. The design of the axial substituents in compounds **1a–c** is derived from a series of silicon Pc (SiPc) derivatives, bearing two of the same substituents at the axial positions of their silicon atom, described by some of us and which previously showed activatable photodynamic properties.[31] These substituents include: (i) a bulky pyrene-containing hydrophobic group, where the pyrene moiety could be used as an additional fluorophore (**1a**); (ii) an amino group with two methoxy(triethylenoxy) axial chains for increasing hydrophilicity (**1b**); and (iii) a reference hydrophobic group that lacks the bulky pyrene unit (**1c**). Importantly, the rationale of the present study is to extend the interesting photodynamic activity of that SiPc-based series to compounds **1a–c**, where the SubPc platform provides an additional, outstanding potential for fluorescence imaging that Pcs just do not have. Consequently, we have developed an in-depth 2D and 3D in vitro study of SubPcs **1a–c** for fluorescence imaging of and PDT against HeLa, SCC-13, and A431 cancer cell lines. The selection of these cell lines is based on the fact that they all represent examples of superficial human cancers (cervix, skin, and vulva, respectively) in which PDT can be applied and, therefore, the type of lesions that could effectively be targeted by SubPcs without decreasing their activity due to tissue light absorption and scattering effects. Results from these studies show that the three PS derivatives (**1a**, **1b**, and **1c**) are able to enter into these tumor cells, grown in monolayer (2D) or in spheroids (3D), inducing in both cases a strong fluorescence, in lysosomes or vacuoles (endosomes) depending on the SubPc axial substituent, under green light irradiation. Moreover, for the most efficient dual-role PS (**1a** and **1c**), preliminary in vivo studies in mice provide proof-of-concept of their promising therapeutic action.

2. Results and Discussion

2.1. Synthesis of SubPcs 1a–c

SubPcs **1a–c** were synthesized from SubPcBCl (**Scheme 1**), the synthesis of which was previously described.[28] To allow for axial substitution with nucleophiles **2–4**,[31] SubPcBCl was transformed into the reactive SubPc–triflate intermediate, following a successful substitution procedure developed previously in our research group.[32] To this end, SubPcBCl was first dissolved in dry toluene and treated with 1.2 equiv. of silver triflate, to irreversibly remove the axial chlorine atom and to obtain a "SubPcB$^+$" species with a weakly coordinating triflate anion. The formation of this triflate intermediate was followed by thin layer chromatography and usually completes after ≈40 min of reaction at room temperature. The activated SubPc–triflate intermediate shows considerable reactivity toward nucleophilic attack at the boron atom, and can be easily reacted with a variety of nucleophiles. Therefore, upon completion of the formation of the triflate intermediate, 2 equiv. of the corresponding nucleophile (i.e., compound **2**, **3**, or **4**) were added to the reaction mixture, in the presence of 1.2 equiv. of freshly distilled *N*,*N*-diisopropylethylamine (DIPEA) to

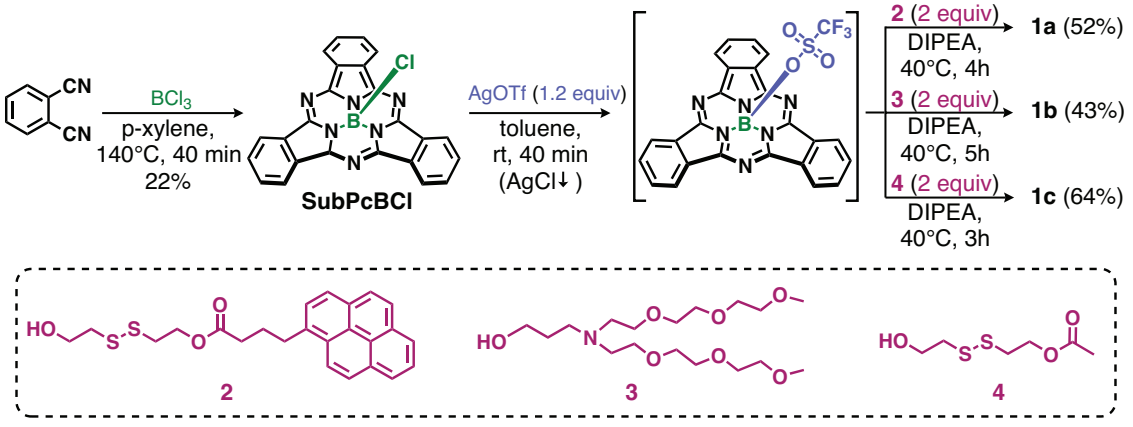

Scheme 1. Scheme of the synthetic route toward SubPcs **1a–c**.

neutralize the triflic acid generated in this step, which could promote unwanted side reactions. The reaction has to be performed under strictly anhydrous conditions, as the presence of water traces immediately leads to a mixture of hydroxy-SubPc and the μ-oxo dimer.[32] The resulting SubPcs **1a–c** could be easily purified by column chromatography, generally using toluene/tetrahydrofuran (THF) mixtures of different polarities as the eluent. A second purification step by size exclusion chromatography (SEC), with Bio-Beads as the stationary phase and toluene as the eluent, was performed to remove any traces of free alcohol or μ-oxo dimer. In this way, SubPcs **1a–c** were obtained with moderate yields, ranging from 43% to 64% (see Supporting Information for the complete procedures).

2.2. Spectral Features and Photophysical Properties

The normalized absorption spectra of SubPcs **1a–c**, measured in dimethylformamide (DMF) (Figure S1, Supporting Information), show the typical and intense Q band, at 566 nm for SubPcBCl and at 562 nm for the axially substituted SubPcs **1a–c**, which indicates that they are nonaggregated. Besides, they all present the typically broad Soret band, with a maximum around 305 nm. For SubPc **1a**, additional absorption bands at 329 and 345 nm can be distinguished, characteristic of the axial pyrene moiety. Exact values of the electronic absorption features for each SubPc can be found in **Table 1**. Upon excitation at 345 nm, all the SubPcs showed a fluorescence emission around 571 nm (F_{571}), varying in intensity, with the pyrene-bearing compound **1a** also showing a small emission band around 377 nm (F_{377}). The ϕ_F values for both the SubPc and pyrene moieties were determined in DMF, relative to F_{12}SubPcBCl in benzonitrile (ϕ_F = 0.58) and anthracene in cyclohexane (ϕ_F = 0.36), exciting at 520 or 345 nm, respectively (Table 1). As main conclusion, the ϕ_F of the three SubPcs **1a–c** were high (≈0.3–0.6), encouraging their use for optical imaging. Besides, the emission of the pyrene unit from SubPc **1a** is quenched (ϕ_F = 0.02), probably caused by an electronic energy transfer between the pyrene moiety and the SubPc core due to partial overlap of the pyrene emission spectrum with the SubPc Q-band, yet electron transfer cannot in principle be ruled out.[31] The photosensitizing efficiency of SubPcs **1a–c**, on the other hand, was evaluated by determining their ϕ_Δ in DMF following the well-known relative method, based on the photoinduced decomposition of the chemical scavenger 1,3-diphenylisobenzofuran (Figure S2, Supporting Information), which reacts readily with $^1O_2$ (Table 1).[33] From this data it can be inferred that the three SubPcs are efficient $^1O_2$ generators, with ϕ_Δ values between 0.37 and 0.56. The SubPc **1a** is a particularly good PS, equaling the photodynamic capacity of nonsubstituted ZnPc, which was used as the reference compound.

Table 1. Electronic absorption and photophysical data for SubPcBCl and the SubPcs **1a–c** in DMF.

Compound	λ_{max} [nm]	λ_{em} [nm][a)]	ϕ_{F377} [%][b)]	ϕ_{F571} [%][c)]	ϕ_Δ [%][d)]
SubPcBCl	566	575	–[e)]	55	47
1a	562	571	2	38	56
1b	562	571	–[e)]	29	37
1c	562	571	–[e)]	36	49

[a)]Excited at 520 nm; [b)]Excited at 345 nm, using anthracene in cyclohexane as the reference compound (ϕ_F = 0.36); [c)]Excited at 520 nm, using F_{12}SubPcBCl in benzonitrile (ϕ_F = 0.58) as the reference compound; [d)]Using ZnPc in DMF as the reference compound (ϕ_Δ = 0.56); [e)]Not applicable, because the compound does not contain any pyrene moiety.

2.3. Subcellular Localization of SubPcs 1a–c

As the subcellular localization of a PS can determine its efficiency for PDT, as well as the type of cell death,[34,35] the distribution of SubPcs **1a–c** within SCC-13 and HeLa cells was carefully evaluated by fluorescence microscopy, performing co-localization studies with fluorescent markers for specific organelles. To this end, cells were incubated for 18 h with SubPcs **1a–c** at a concentration of 2×10^{-6} M, and subsequently further incubated with LysoTracker, MitoTracker, or NBD C_6-ceramide probes. For both cell types, a similar intracellular distribution of SubPcs **1a–c** could be observed, as determined by their red fluorescence emission observed under green light excitation (**Figure 2**; Figure S3, Supporting Information). After incubation with SubPc **1a**, the two cell lines, grown in monolayer, showed an intense granular red fluorescence emission around the nucleus, as well as in a yuxtanuclear position (Figure 2A, left). This intracellular emission of SubPc **1a** was coincident with that of the lysosomes, since a yellowish fluorescence due to the overlapping of red and green emission (from the SubPc and LysoTracker®, respectively) was observed. Such fluorescence was clearly different from that of the mitochondrial and Golgi signal patterns. Identical results were obtained with SubPc **1b** (Figure S3, Supporting Information). SubPc **1c**, on the contrary, showed a strong granular (vacuolar) red fluorescence emission localized also around the nucleus and nearby but not coincident with lysosomes, neither with mitochondria nor with the Golgi apparatus (Figure 2A, right). Control cells (without PS incubation) showed a very low emission, which corresponds to mitochondrial autofluorescence (not shown), confirming that the fluorescence detected in SCC-13 and HeLa was indeed due to intracellular accumulation of the SubPc dyes.

In addition, and taking into account that tumor spheroids are considered to be a better model to mimic the in vivo situation than monolayers of tumor cells, with regard to tumor shape,[36,37] we then evaluated the ability of the SubPcs **1a–c** to penetrate into these tumor like structures formed from SCC-13 and HeLa cells (Figure 2B). As revealed by the intense emission observed under the fluorescence microscope, SubPcs **1a–c** effectively entered into the spheroids: SubPc **1a** localized in the lysosomes (identical localization was observed for SubPc **1b**, not shown), whereas SubPc **1c** presented a granular localization pattern nearby but not inside the lysosomes. From these observations, we can conclude that SubPcs **1a** and **1b** exhibit the same localization pattern in 2D and 3D in vitro localization experiments, both in SCC-13 and HeLa cells, being localized in lysosomes, whereas SubPc **1c** seems

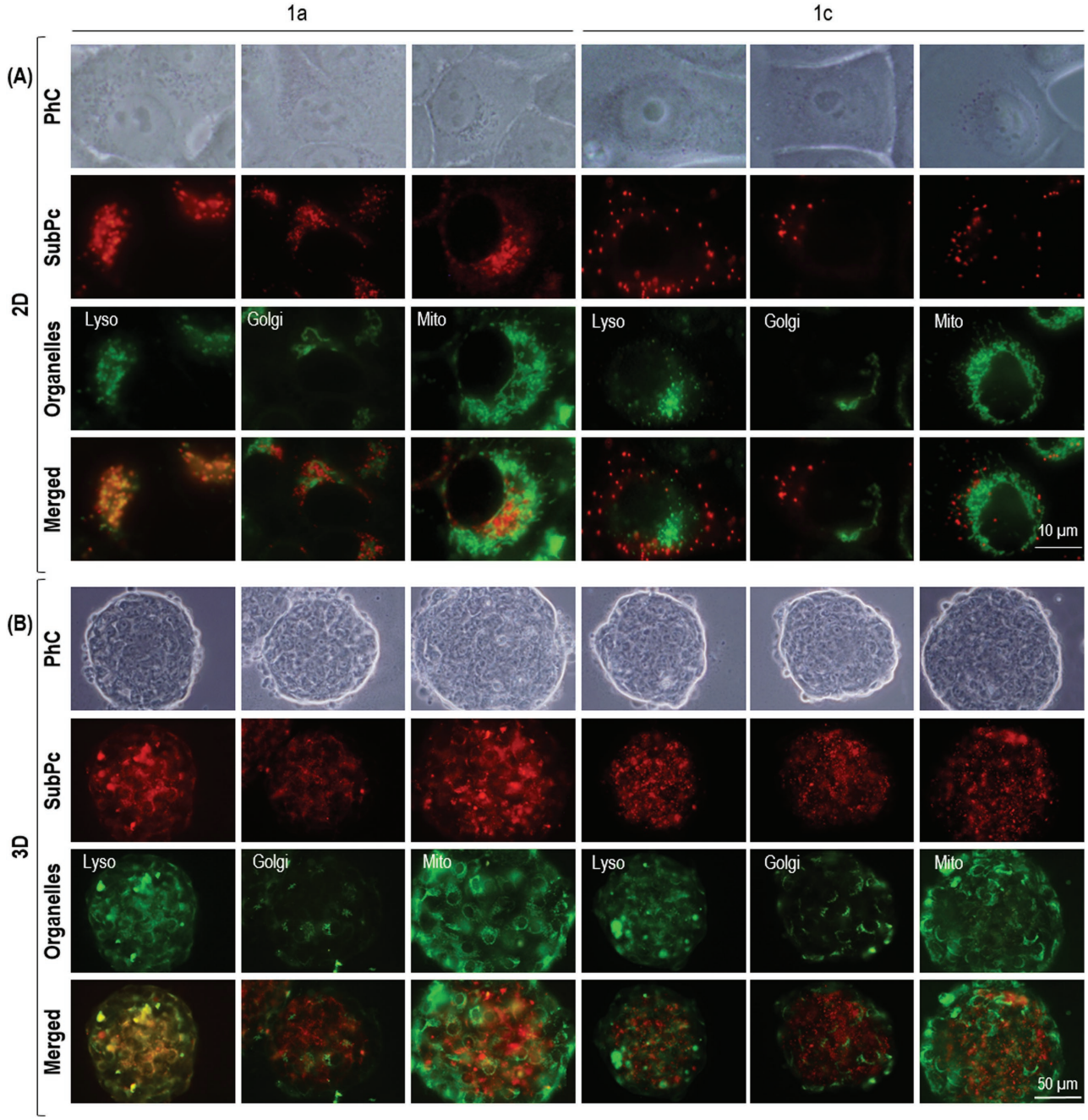

Figure 2. Subcellular localization of SubPc **1a** and SubPc **1c** in A) 2D cultures and B) 3D cultures of SCC-13 cells after 18 h of incubation. Experiments with cultures of HeLa cells gave identical results (not shown). Phase contrast (PhC). Red fluorescence is from SubPcs and green fluorescence is from lysosomes (Lyso), Golgi apparatus (Golgi), and mitochondrial (Mito). The merged image shows the green and red fluorescence together. A blue (450–490 nm) exciting lamp was used for LysoTracker and MitoTracker or NBD C_6-ceramide probes, while green (545 nm) exciting light was utilized for SubPcs.

to present vacuolar (endosomal) localization. This is interesting because the subcellular localization of a PS is closely related to the cell death mechanism induced by PDT, as a consequence of the short life time of $^1O_2$, the main reactive species produced after PDT, for which the primary localization of the PS determines the initial subcellular damage upon its activation.[38,39] Besides, given that no differences were detected between the SCC-13 and HeLa cells, localization seems to be mainly related to the molecular structure of the SubPc employed, for which repeating the subcellular localization experiments in A431 cells was considered not necessary.

2.4. Phototoxicity Experiments and ROS Production

The phototoxicity of SubPcs **1a–c** upon green light irradiation was evaluated by the 3-(4,5-dimethylthiazol-2-yl)-2,5-diphenyltetrazolium bromide (MTT) assay in SCC-13, HeLa, and

Table 2. Toxicity effects in SCC-13, HeLa, and A431 cells induced by green light, in the absence of any SubPc, and by incubation with SubPcs **1a–c** in the dark. Cell toxicity was evaluated by the MTT assay 24 h after treatment. Data are expressed as mean values obtained from three independent experiments ± standard deviation (SD).

Compound	Concentration[M]	Surviving fraction (% ± SD)		
		SCC-13	HeLa	A431
Control		100 ± 4.8	100 ± 4.4	100 ± 4.0
4.7 J cm^{-2}		99 ± 1.5	100 ± 3.0	95 ± 2.1
1a	2×10^{-6}	101 ± 3.6	102 ± 4.7	95 ± 2.0
	5×10^{-8}	103 ± 3.4	99 ± 1.9	96 ± 2.5
1b	2×10^{-6}	102 ± 4.6	104 ± 1.5	103 ± 1.1
	5×10^{-8}	102 ± 2.4	98 ± 3.0	103 ± 6.8
1c	2×10^{-6}	95 ± 2.9	96 ± 2.9	92 ± 2.4
	5×10^{-8}	100 ± 1.5	98 ± 3.5	94 ± 1.0

A431 cells, grown in monolayer. For this purpose, we first evaluated the inherent toxicity of two different concentrations of the three SubPcs (2×10^{-6} and 5×10^{-8} M) in cells after 5 h of incubation in presence of PS in the dark and, separately, in the absence of PS after the administration of different green light doses (2–4.7 J cm^{-2}). The results obtained, shown in **Table 2**, indicate that none of these SubPc concentrations, neither the administration of green light, induced significant cytotoxic effects in the cell lines studied, and survival rates above 92% were obtained. We then continued to evaluate the photodynamic activity of the three SubPcs toward SCC-13, HeLa, and A431 cells upon irradiation.[40] For the photodynamic treatments, we selected the lower noncytotoxic SubPc concentration (i.e., 5×10^{-8} M) and, after 5 h of incubation, cells were exposed to different green light doses (2, 3.35, and 4.7 J cm^{-2}). For both PDT treatments with SubPc **1a** and **1c**, a drastic decrease in cell survival was revealed for the three cell lines (**Figure 3**A–C), in line with the light dose employed.

SubPc **1c** is a more efficient PS than **1a**, according to the statistically significant differences in performance observed between them. The measured cell survival values are actually comparable to those of other PS used in PDT, such as LDH-ZnPcS8,[41] or silicaCe6-FA.[42] SubPc **1b**, in turn, was not effective for PDT at this concentration, since the cell survival values obtained after photodynamic treatments were similar to those observed in untreated control cells. When higher concentrations of SubPc (i.e., 0.1×10^{-6} M) were employed, however, a significant decrease in cell survival was detected, even for SubPc **1b** (Figure S4A, Supporting Information). Importantly, the observed cell survival values find correspondence to the capacity of the three SubPc dyes as $^1O_2$ generators (Table 1). Altogether, the results also indicate that HeLa cells were more resistant to photodynamic treatments with these SubPcs than SCC-13 and A431 cells (Figure S4B, Supporting Information). The cell morphology of the treated cells was also analyzed 24 h after PDT treatment using phase contrast microscopy (Figure 3D), revealing remarkable changes in the three cell lines. Most cells showed cytoplasmic retraction, with a rounded aspect similar to that of cells in apoptosis,[43] yet elongated cells were also observed in the treated cultures. Interestingly, these images are well correlated with the results obtained from cell viability assays.

We next analyzed by fluorescence microscopy the intracellular ROS formation in HeLa, SCC-13, and A431 cells, when subjected to PDT with the SubPc **1a** or **1c**, using for this purpose the DHF-DA fluorescent probe (Figure S5, Supporting Information). As shown in Figure S5A (Supporting Information), controls presented very low green florescent signal due to moderate endogenous production of ROS.[44] Similarly, cells incubated with SubPcs in dark conditions showed a very low green fluorescence. In contrast, cells subjected to PDT showed an intense fluorescence in all cell types, compared to baseline levels, revealing a prominent ROS production after the photodynamic treatment. Fluorescence values after PDT were actually significantly higher than for dark SubPc treatments ($P < 0.005$) (Figure S5B, Supporting Information).

Given the results obtained in cells grown in monolayer, we next evaluated the photodynamic activity of SubPcs **1a** and **1c** in A431 spheroids. For the PDT treatments, we selected the highest noncytotoxic SubPc concentration (2×10^{-6} M), 5 h of incubation, and a 4.7 J cm^{-2} light dose. For both treatments, with SubPc derivatives **1a** and **1c**, a significant decrease in spheroid diameter can be observed 24 h after treatment (**Figure 4**A). In addition, the acridine orange/ethidium bromide (AO/EB) staining method revealed that the treated spheroids were formed by damaged cells (fluorescing in orange/red) while controls were formed by viable cells (fluorescing in green) (Figure 4B). Therefore, we can conclude that both SubPcs were photodynamically active also in the 3D in vitro model.

2.5. In vivo Studies

Preliminary in vivo studies were performed to confirm the imaging and therapeutic potential of the SubPcs under study. As a proof-of-concept for imaging, we tested if it is possible to capture the fluorescence of these PS in vivo. In particular, 0.2 mL of 2×10^{-6} M SubPc in phosphate-buffered saline (PBS) were injected subcutaneously on the back flank of a mice (CD-1, shaved of the back dorsal skin using a hair clipper), and the resulting fluorescence was immediately evaluated by the IVIS Lumina system (λ_{exc} = 450 nm, λ_{em} = 580 nm). Following this simple, nonoptimized protocol, Figure S6 (Supporting Information) shows an image where the emission of compound **1a**, as an example, can be clearly identified (see white arrow), demonstrating that the fluorescence of SubPc dyes can be detected in vivo, and the skin is not a barrier to observe the compound.

To evaluate the therapeutic capacity of SubPcs **1a** and **1c**, on the other hand, A431 cells were subcutaneously injected in both flanks of mice and when the tumors reached a size between 5 and 7 mm of diameter, treatments were applied. No evident differences were observed in the size of tumors exposed only to light or with injected SubPc **1a** or **1c** (nonirradiated); therefore, all were grouped and shown as "controls." For PDT treatments, the SubPcs **1a** or **1c** were administered by intratumoral injection

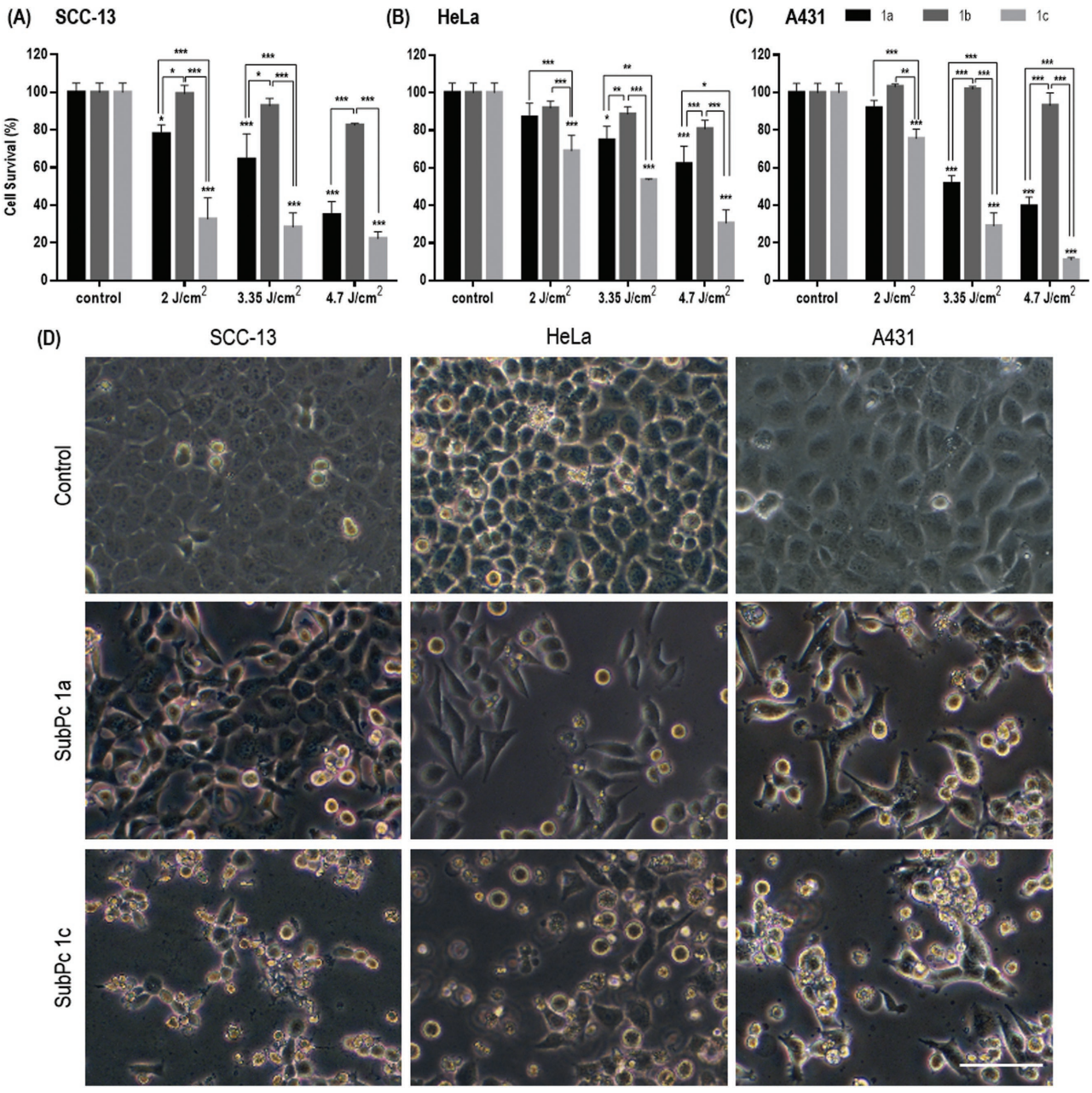

Figure 3. Surival of A) SCC-13, B) HeLa, and C) A431 cells after photodynamic treatment with SubPcs **1a–c** (5×10^{-8} M, 5 h of incubation followed by different light doses: 2, 3.35, and 4.7 J cm^{-2}). Cell survival was evaluated 24 h after photodynamic treatment by the MTT assay. Each point corresponds to the mean value ± SD obtained from three independent experiments. D) Morphological changes observed in SCC-13, HeLa, and A431cells 24 h after PDT with the SubPcs **1a** and **1c** (0.05×10^{-6} M, 5 h of incubation followed by a green light dose of 4.7 J cm^{-2}). Scale bar: 50 µm. *$P < 0.05$, **$P < 0.01$, ***$P < 0.005$.

and, 2 h later, exposed to 12 J cm^{-2} of green light (**Figure 5**A). Treated tumors showed a size smaller than that of controls, as could be observed by visual inspection (Figure 5B) and confirmed after measuring them (Figure 5C). Reduction in tumor size was observed already 2 d after treatment, compared to controls not subjected to PDT. Tumors were subjected to a second PDT treatment and a greater decrease in their sizes was detected. The histological analysis of the tumors revealed no differences between the tumors with one or two PDT-treatments (not shown). The H&E staining showed an increment of red blood cell extravasation with progression to coagulative epidermal necrosis in tumors after SubPc injection and PDT (Figure 5D), this being related to the observed smaller size of treated tumors. Therefore, both SubPcs are able to damage tumors cells upon green light irradiation.

3. Conclusions

In sum, in this article we have demonstrated for the first time, with in vitro and in vivo experiments, that SubPcs present a

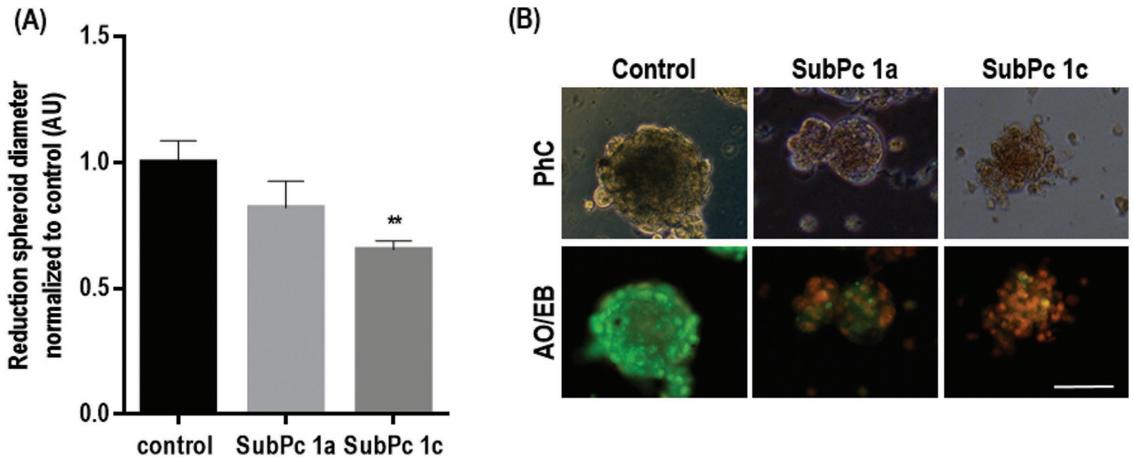

Figure 4. Photodynamic activity of SubPc **1a** and **1c** in A431 spheroids. A) Reduction in spheroid diameters 24 h after PDT treatment with SubPcs **1a** and **c** (2×10^{-6} M, 5 h of incubation and 4.7 J cm^{-2} of green light). Diameters were measured using the Image J software and normalized to size control. Each point corresponds to the mean value ± SD obtained from three independent experiments. B) 24 h after photodynamic treatment the spheroids were labeled with acridine orange (AO) and ethidium bromide (EB) to determine viable (green) or damage spheroids (orange). Scale bar: 50 µm. $^{**}P < 0.01$.

promising dual potential for optical imaging and PDT of superficial cancers. This opens a window of opportunity for these optoelectronic dyes, whose application in biomedical research has, until now, remained clearly underexplored. The main advantages of SubPcs in this respect include their high fluorescence and singlet oxygen quantum yields, and their nonplanar aromatic structure, which allows fine-tuning of the aggregation and excited state properties of these macrocycles by adequately designed axial substitution. Within the series of compounds studied herein, for example, different subcellular localization can be observed and related to the different SubPc axial substituents, an effect that we tentatively ascribe to their different aggregation behavior in the biological medium. Although the structure–property relationships for this family of PS has to be clarified in further studies, their excellent capacity to perform both imaging and therapeutic functions that are triggered only by light represents a very promising approach within the field of theranostics.

4. Experimental Section

Materials and Methods: All reagents were used as purchased from commercial sources without further purification. Solvents were dried using standard techniques prior to use. The starting materials silicon phthalocyanine dichloride ($SiPcCl_2$), 1-pyrene butyric acid, 2-hydroxyethyl disulfide, triethylene glycol monomethyl ether, and 3-amino-1-propanol were commercially available. Nucleophiles **2**, **3**, and **4** were previously synthesized.[31]

General Procedure for the Axial Substitution of SubPcBCl: SubPcBCl (0.08 g, 0.19 mmol) and silver triflate (0.06 g, 0.23 mmol) were dissolved in anhydrous toluene (3 mL) and the mixture was stirred at room temperature under argon atmosphere for 40 min until SubPcBCl was consumed. Once the SubPc–triflate intermediate is generated, the nucleophile R–OH (**2**, **3**, or **4**) (0.38 mmol) and DIPEA (40 µL, 0.23 mmol) were added. The mixture was stirred at 40 °C until the reaction was completed. The solvent was removed by evaporation under reduced pressure and the product was directly purified by column chromatography on silica gel using mixtures of toluene and THF as the eluent. Further specific purification steps for each SubPc are detailed in the Supporting Information.

Cell Cultures: For in vitro studies, we used the following human tumoral cell lines: SCC-13 (squamous cell carcinoma from face), HeLa (cervical adenocarcinoma), and A431 (squamous cell carcinoma from vulva). Cell lines were grown in DMEM (Dulbecco's modified Eagle's medium high glucose 1×) supplemented with 10% (v/v) fetal bovine serum (FBS), 50 units mL^{-1} penicillin, and 50 µg mL^{-1} streptomycin, all from Thermo Fisher Scientific Inc. Cell cultures were performed under standard conditions of 5% CO_2, 95% of humidity, and 37 °C of temperature and propagated by trypsinizing cultures with 1×10^{-1} M EDTA/0.25% Trypsin (w/v).

Spheroid Cultures: Spheroids were grown from SCC-13, HeLa, and A431 cells using specific medium containing DMEM/F12 (1:1) (F-12 Nutrient Mixture, Ham, Gibco), 2% B27 serum free supplement (17504-044, Gibco), 20 ng mL^{-1} EGF (E4269, Sigma), 0.4% bovine serum albumin (A7906, Sigma), and 4 µg mL^{-1} insulin (41400-045, Gibco). The cells were plated at 15 000 cells mL^{-1} per well precoated with 1.2% poly-HEMA (2-hydroxyethyl methacrylate, Sigma). The spheroids were formed after 6 d of culture.

Photosensitizer Incubation: Stock solutions of the SubPcs **1a–c** (1.5×10^{-3} M) were prepared in dimethyl sulfoxide (DMSO) and work solutions were obtained in DMEM without FBS. The final concentration of DMSO was always lower than 0.5% (v/v) and the lack of toxicity of such concentration for the cells was confirmed. All the treatments were performed when cultures reached around 60–70% of confluence.

Subcellular Localization: To analyze the intracellular localization of SubPcs, SCC-13 and HeLa cells were grown on coverslips and, incubated with SubPcs **1a–c** to a final concentration of 2×10^{-6} M for 18 h at 37 °C. After incubation, cells were further incubated for another 30 min with known fluorescent probes for lysosomes (LysoTracker Green DND-26, Invitrogen), mitochondria (MitoTracker Green FM, Invitrogen), or Golgi apparatus (NBD, C_6-ceramide (*N*-[6-[(7-nitro-2-1,3-benzoxadiazol-4-yl)amino]hexanoyl]- D-erythro-sphingosine, Invitrogen)) at the concentrations indicated by the suppliers. Then, cells were briefly washed in PBS, mounted on slides with a drop of PBS and immediately observed under the fluorescence microscope.

Photodynamic Treatment: Monolayers of SCC-13, HeLa, and A431 cells grown in 24-well plates were incubated with different concentrations of SubPcs, ranging from 0.05×10^{-6} M to 2×10^{-6} M (in DMEM without FBS) for 5 h. Subsequently, cells were irradiated with a green light emitting diode source ($\lambda = 525$ nm, the irradiance at the cell culture position was 11.1 mW cm^{-2}) for variable doses, ranging from 2 to 4.7 J cm^{-2}. After irradiation, cells were further incubated in complete medium at 37 °C for 24 h until evaluation. Spheroids were also treated in the same conditions used for the monolayers. Dark control experiments were carried out in

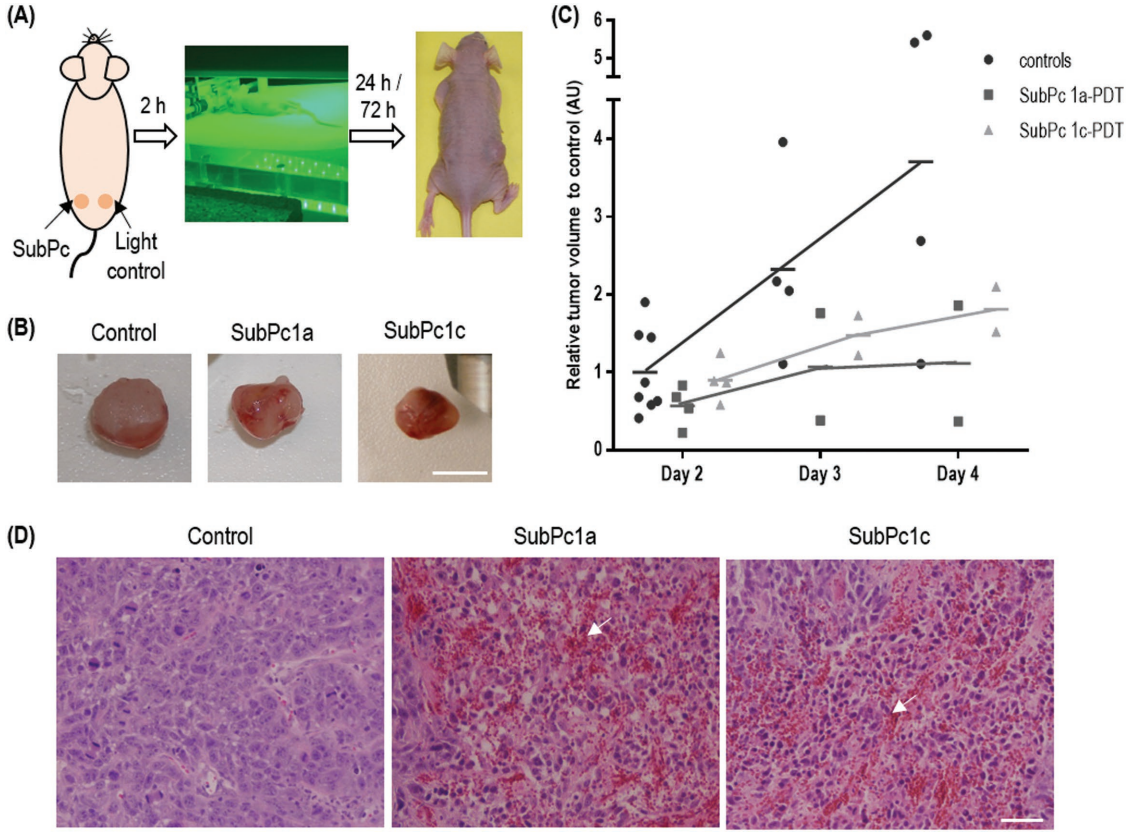

Figure 5. In vivo studies. A) A-431 cells were injected in both right and left flanks of athymic nude mice. When the tumors reached a size between 5 and 7 mm of diameter, the tumors received 0.2 mL of 2×10^{-6} M SubPc **1a** or **1c** by intratumoral injection and, 2 h later, they were exposed to green light with a dose of 12 J cm^{-2}. B) Representative tumors of each group (control, SubPc **1a**-PDT, and SubPc **1c**-PDT), 4 d after the first PDT treatment. C) Tumor volume to relative to control. Each point represents the volume of each tumor calculated as $4/3\pi \times (\text{diameter}/2)^3$. D) Representative photographs of tumor sections stained with H&E 4 d after PDT treatments: control, SubPc **1a**-PDT, and SubPc **1c**-PDT. Scale bar: 50 µm. Arrows indicate extravasated blood in the tumors as a result of SubPc-PDT treatments.

parallel, incubating the cells with the same concentrations of SubPcs, for 5 h in dark. In the same way, to test the effect of green light alone, cells were subjected to different light doses.

Measurement of Intracellular ROS: The intracellular production of ROS in SCC-13, HeLa, and A431 cells was evaluated as previously described.[45] Cells were incubated with SubPc **1a** or **1c** (0.05×10^{-6} M) for 5 h, and in the last hour 2,7-dichloro-dihydrofluorescein diacetate (DHF-DA, Abcam) was added to the cultures, reaching a final concentration of 6×10^{-6} M. Afterward, and without removing DHF-DA, cells were exposed to green light (3.35 J cm^{-2}) and immediately after irradiation analyzed by fluorescence microscopy, under blue excitation light (λ_{exc} = 436 nm). Corresponding controls were performed: cells incubated with DHF-DA without SubPcs nor exposed to green light, and cells incubated with SubPcs and DHF-DA but not exposed to green light. ROS production was quantified by using Image J after measuring green fluorescence.

Morphological Changes and Cellular Toxicity: Changes in general cell morphology after 24 h photodynamic treatments were analyzed by phase contrast microscopy. The toxicity of SubPcs on cells grown in monolayer was evaluated 24 h after photodynamic treatment by the MTT (3-(4, 5-dimethylthiazol-2-yl)- 2, 5-diphenyltetrazolium bromide, Sigma) assay. MTT solution (1 mg mL^{-1}) in PBS was diluted in DMEM (10% FBS) to a final concentration of 50 µg mL^{-1}, added to each well and incubated at 37 °C for 3 h. After incubation, the formazan crystals were dissolved in DMSO and the absorbance at 542 nm was measured by spectrophotometry (Espectra Fluor 4, Tecan). Cellular toxicity was expressed as cell survival percentage of control (cell survival (%) = (mean OD value of PDT-treated cells/mean OD value of control cells) × 100%). The cellular toxicity in spheroids was evaluated by measuring their diameters using the Image J software, and by using two fluorescent dyes that bind to cells) DNA, acridine orange (stain both live and dead cells in green) and ethidium bromide (stain only cells that have lost membrane integrity in red).[46]

Tumor Xenograft Study: For in vivo study, we used eight hairless athymic nude mice from 6 to 8 weeks (BALB/cByJ-Hfh11nu; Charles River). Mice were housed and maintained under specific pathogen free conditions and provided with food and water ad libitum. All the experimental procedures with animals were carried out in compliance with the guidelines in RD 53/2013 (Spain) and was approved by the Ethics Committee from Consejo Superior de Investigaciones Científicas (CSIC) and Comunidad Autonoma of Madrid (CAM, Consejería de Medio Ambiente; Register number: ES80790000188) in the frame of the project FIS-PI15/00974 supported by the Spanish Ministerio de Economía y Competitividad. Monolayer cultures of A-431 cells were trypsinized, resuspended in PBS and 2×10^6 cells were subcutaneously injected in both, right and left flanks of the animals. Mice were monitored for the appearance of tumors and treated when they reached a size between 5 and 7 mm of diameter (calculated from caliper measurements). The tumors were distributed as follows: 4 control light; 2 SubPc **1a** (unirradiated); 2 SubPc **1c** (unirradiated); 4 SubPc **1a**-PDT; and 4 SubPc **1c**-PDT. For PDT treatments, mice received 0.2 mL of 2×10^{-6} M SubPc **1a** or **1c** by intratumoral injection, and 2 h later, animals were exposed to 12 J cm^{-2} green light by using the emitting diode source situated at 5 cm from the back of the animals. Four mice (half of tumors of each condition) were sacrificed 24 h after the treatments and tumors fixed

in neutral buffered formalin, in included in paraffin, sectioned and stained with hematoxylin and eosin (H&E) for pathological analysis. A second PDT treatment (in the same conditions as the first one) was administered to the tumors. The mice were then sacrificed and the tumors harvested for the same pathological analysis.

Microscopy and Statistical Analysis: Microscopic observations were carried out using an Olympus BX61 epifluorescence microscope, equipped with a HBO 100 W mercury lamp and the corresponding filter sets for fluorescence microscopy: blue (450–490 nm, exciting filter BP 490), and green (545 nm, exciting filter BP 545). Photographs were obtained with digital camera Olympus DP50 and processed using Adobe PhotoShop CS5 extended version 12.0 software (Adobe Systems Inc., USA). Data are expressed as the mean value ± standard deviation (SD) of at least three independent experiments. The statistical significance was determined using one-way ANOVA followed by Tukey's test. A *P*-value lower than 0.05 was considered as significant.

Supporting Information

Supporting Information is available from the Wiley Online Library or from the author.

Acknowledgements

E.v.d.W. and M.M. contributed equally to this work. The research leading to these results has received funding from the People Programme (Marie Curie Actions) of the European Union's Seventh Framework Program FP7-PEOPLE-2012-ITN under REA grant agreement No. GA 316975. AdlE holds a Ramón y Cajal contract from the Spanish Ministry of Economy (MINECO). This work was supported by EU (CosmoPHOS-nano, FP7-NMP-2012-6, 310337-2; GLOBASOL, FP7-ENERGY-2012-J, 309194-2), the Spanish MINECO (CTQ-2014-52869-P (TT) and CTQ-2014-53673-P (AdlE)), CAM (FOTOCARBON, S2013/MIT-2841), grants from Instituto de Salud Carlos III, MINECO and Feder Funds (PI15/00974) and by S2010/BMD-2359 from Comunidad de Madrid.

Conflict of Interest

The authors declare no conflict of interest.

Keywords

cancer, optical imaging, photodynamic therapy, subphthalocyanine dyes

Received: October 13, 2017
Revised: November 21, 2017
Published online:

[1] E. K. Lim, T. Kim, S. Paik, S. Haam, Y. M. Huh, K. Lee, *Chem. Rev.* **2015**, *115*, 327.
[2] H. Chen, W. Zhang, G. Zhu, J. Xie, X. Chen, *Nat. Rev. Mat.* **2017**, *2*, 17024.
[3] X. Ai, J. Mu, B. Xing, *Theranostics* **2016**, *6*, 2439.
[4] I. Johnson, in *Optical Imaging of Cancer*, (Eds.: E. Rosenthal, K. R. Zinn), Springer, New York **2010**, p. 59.
[5] M. H. Abdel-Kader, *Photodynamic Therapy – From Theory to Application*, Springer, Heidelberg, Germany **2014**
[6] M. Wainwright, T. Maisch, S. Nonell, K. Plaetzer, A. Almeida, G. P. Tegos, M. R. Hamblin, *Lancet Infect. Dis.* **2017**, *17*, e49.
[7] S. Nonell, C. Flors, *Singlet Oxygen: Applications in Biosciences and Nanosciences*, RSC Publishing, Cambridge, UK **2016**.
[8] J. F. Lovell, T. W. B. Liu, J. Chen, G. Zheng, *Chem. Rev.* **2010**, *110*, 2839.
[9] M. Ethirajan, Y. Chen, P. Joshi, R. K. Pandey, *Chem. Soc. Rev.* **2011**, *40*, 340.
[10] C. G. Claessens, A. David González-Rodríguez, T. Torres, *Chem. Rev.* **2002**, *102*, 835.
[11] J. A. A. W. Elemans, R. Van Hameren, R. J. M. Nolte, A. E. Rowan, *Adv. Mater.* **2006**, *18*, 1251.
[12] J. W. Ryan, E. Anaya-Plaza, A. de la Escosura, T. Torres, E. Palomares, *Chem. Commun.* **2012**, *48*, 6094.
[13] V. V. Roznyatovskiy, C.-H. Lee, J. L. Sessler, *Chem. Soc. Rev.* **2013**, *42*, 1921.
[14] H. Lu, N. Kobayashi, *Chem. Rev.* **2016**, *116*, 6184.
[15] T. Basova, A. Hassan, M. Durmus, A. G. Gürek, V. Ahsen, *Coord. Chem. Rev.* **2016**, *310*, 131.
[16] N. Nishiyama, A. Iriyama, W.-D. Jang, K. Miyata, K. Itaka, Y. Inoue, H. Takahashi, Y. Yanagi, Y. Tamaki, H. Koyama, K. Kataoka, *Nat. Mater.* **2005**, *4*, 934.
[17] F. Dumoulin, M. Durmuş V. Ahsen, T. Nyokong, *Coord. Chem. Rev.* **2010**, *254*, 2792.
[18] D. K. P. Ng, *Future Med. Chem.* **2014**, *6*, 1991.
[19] J. Mikkila, E. Anaya-Plaza, V. Liljestrom, J. R. Caston, T. Torres, A. de la Escosura, M. Kostiainen, *ACS Nano* **2016**, *10*, 1565.
[20] J. A. Gonzalez-Delgado, P. J. Kennedy, M. Ferreira, J. P. C. Tome, B. Sarmento, *J. Med. Chem.* **2016**, *59*, 4428.
[21] E. Anaya-Plaza, E. van de Winckel, J. Mikkila, J.-M. Malho, O. Ikkala, O. Gulias, R. Bresoli-Obach, M. Agut, S. Nonell, T. Torres, M. A. Kostiainen, A. de la Escosura, *Chem. Eur. J.* **2017**, *23*, 4320.
[22] C. G. Claessens, D. González-Rodríguez, M. S. Rodríguez-Morgade, A. Medina, T. Torres, *Chem. Rev.* **2014**, *114*, 2192.
[23] Y. Bernhard, P. Winckler, R. Chassagnon, P. Richard, É. Gigot, J.-M. Perrier-Cornet, R. A. Decréau, *Chem. Commun.* **2014**, *50*, 13975.
[24] Y. Bernhard, P. Winckler, J.-M. Pierrer-Cornet, R. A. Decreau, *Dalton Trans.* **2015**, *44*, 3200.
[25] K. J. McAuliffe, M. A. Kaster, R. G. Szlag, E. R. Trivedi, *Int. J. Mol. Sci.* **2017**, *18*, 1177.
[26] H. Xu, X.-J. Jiang, E. Y. M. Chan, W.-P. Fong, D. K. P. Ng, *Org. Biomol. Chem.* **2007**, *5*, 3987.
[27] M. Spesia, E. Durantini, *Dyes Pigm.* **2008**, *77*, 229.
[28] C. G. Claessens, D. González-Rodríguez, B. del Rey, T. Torres, G. Mark, H.-P. Schuchmann, C. von Sonntag, J. G. MacDonald, R. S. Nohr, *Eur. J. Org. Chem.* **2003**, *14*, 2547.
[29] M. E. El-Khouly, A. El-Refaey, W. Nam, S. Fukuzumi, Ö. Göktuğ, M. Durmuş, *Photochem. Photobiol. Sci.* **2017**, *11*, 107.
[30] N. Shibata, B. Das, E. Tokunaga, M. Shiro, N. Kobayashi, *Chem. Eur. J.* **2010**, *16*, 7554.
[31] E. van de Winckel, R. J. Schneider, A. de la Escosura, T. Torres, *Chem. A Eur. J.* **2015**, *21*, 18551.
[32] J. Guilleme, D. González-Rodríguez, T. Torres, *Angew. Chem., Int. Ed.* **2011**, *50*, 3506.
[33] S. Makhseed, A. Tuhl, J. Samuel, P. Zimcik, N. Al-Awadi, V. Novakova, *Dye. Pigment.* **2012**, *95*, 351.
[34] Y. J. Hsieh, C. C. Wu, C. J. Chang, J. S. Yu, *J. Cell. Physiol.* **2003**, *194*, 363.
[35] J. J. Chen, L. J. Gao, T. J. Liu, *Oncol. Lett.* **2016**, *11*, 775.
[36] W. Mueller-Klieser, *Am. J. Physiol., Cell Physiol.* **1997**, *273*, C1109.
[37] T. B. Andersson, *Basic Clin. Pharmacol. Toxicol.* **2017**, *121*, 234.
[38] J. Xu, F. Zeng, H. Wu, C. Hu, S. Wu, *Biomacromolecules.* **2014**, *15*, 4249.
[39] G. Kroemer, M. Jäättelä, *Nat. Rev. Cancer.* **2005**, *5*, 886.
[40] L. B. de Paula, F. L. Primo, A. C. Tedesco, *Biophys. Rev.* **2017**, *9*, 1.
[41] C. Li, B. Y. Zheng, M. R. Ke, Y. Zhang, J. D. Huang, J. Yoon, *Theranostics.* **2017**, *7*, 2746.

[42] S. Bharathiraja, M. S. Moorthy, P. Manivasagan, H. Seo, K.D. Lee, J. Oh, *Photodiagnosis Photodyn. Ther.* **2017**, *19*, 212.
[43] S. Rello, J. C. Stockert, V. Moreno, A. Gámez, M. Pacheco, A. Juarranz, M. Cañete, A. Villanueva, *Apoptosis.* **2005**, *10*, 201.
[44] E. Carrasco, A. Blazquez-Castro, M. I. Calvo, A. Juarranz, J. Espada, *Methods* **2016**, *109*, 180.
[45] A. Blázquez-Castro, E. Carrasco, M. I. Calvo, P. Jaén, J. C. Stockert, A. Juarranz, F. Sánz-Rodríguez, J. Espada, *Cell Biol.* **2012**, *91*, 216.
[46] S. Kasibhatla, G. P. Amarante-Mendes, D. Finucane, T. Brunner, E. Bossy-Wetzel, D. R. Green, *Cold Spring Harb. Protoc.* **2006**, *2006*, pdb-prot4493.